Catalysis Science & Technology

ROYAL SOCIETY OF CHEMISTRY

PAPER

View Article Online
View Journal | View Issue

Cite this: *Catal. Sci. Technol.*, 2025, **15**, 547

Chemical kinetic mechanism for selective catalytic reduction of nitrogen oxides†

Alexey A. Burluka * and Andrew P. Manning ‡

A generic chemical kinetic mechanism for nitric oxide reduction by ammonia is developed exploiting similarities in redox cycles exhibited by different catalysts. The mechanism comprises 28 reactions, the rate constants of which were estimated through analysis of the individual sub-processes and identifying the overall rate with the rate of the limiting step. The chemical kinetics so developed was used to simulate operation of several catalysts in a plug flow reactor. These simulations show that, after taking into account differences in feed gas composition, active site concentration and residence time, varying only one kinetic parameter, namely activation energy for the low-temperature catalytic site oxidation allows one to reconcile the observed differences between copper and iron exchanged zeolites and cerium dioxide with tungsta on titania. Prediction of the NO conversion by vanadia at high temperatures required changes of two kinetic parameters.

Received 9th October 2024,
Accepted 5th December 2024

DOI: 10.1039/d4cy01205d

rsc.li/catalysis

1 Introduction

Removal of nitric oxide from exhaust or flue gas is required for a great variety of applications ranging from a passenger car engine to a large power plant, and selective catalytic reduction (SCR) of NO by ammonia is often the only practical means of achieving this. It is therefore not surprising that there is a wealth of literature, see *e.g.* review of Han *et al.*[1] or Fig. 1 in Lian *et al.*[2] illustrating the exponential growth of the number of publications in recent years, devoted to investigation of SCR surface reactions and their pathways, undertaken through experiments and/or numerical modelling. However, perhaps owing to the complexity and large number of possible transition states, the rate analysis is largely limited to some individual possible reactions with few notable exceptions, *e.g.* Janssens *et al.*[3] Regardless of the exact composition of the catalyst, the SCR proceeds as a cyclic process with two or more interlinked pathways. One of these chemical pathways results in a reduction, during which the catalyst metal lowers the number of its valent bonds and another pathway involves oxidation where the number of valent bonds is restored by reaction with the free oxygen typically present in exhaust or flue gas, *e.g.* Topsøe *et al.*[4] and Han *et al.*[1] The operating temperature of an SCR may also vary from less than 450 K at the cold start to more than 900 K at full load, thus complicating the direct translation of laboratory catalyst kinetic studies, usually performed in a much smaller temperature range, into an applied numerical model.

A number of SCR models represent the processes in terms of net reactions compounding together physisorption, chemical adsorption, surface diffusion and chemical transformations, *e.g.* Olsson *et al.*[5] or De-La-Torre *et al.*[6] In such approaches, the rate

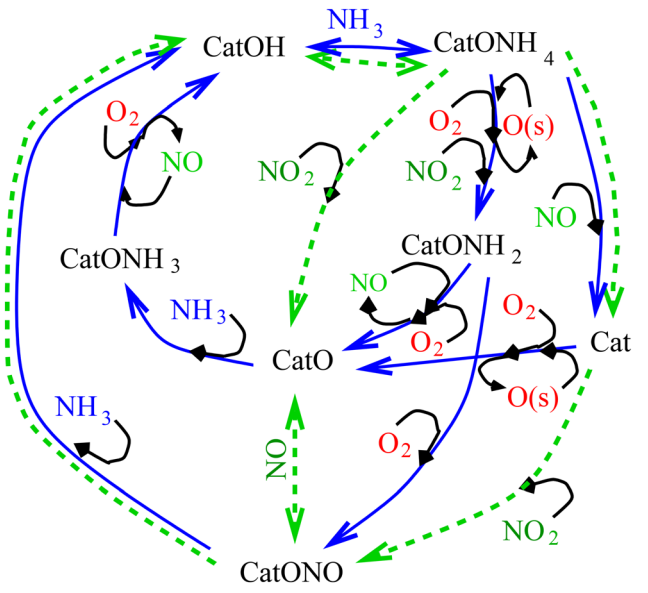

Fig. 1 Graphical representation of the proposed kinetic scheme of selective catalytic reduction of nitric oxide by ammonia.

Department of Mechanical & Construction Engineering, Northumbria University, NE1 8ST, Newcastle-upon-Tyne, UK. E-mail: alexey.burluka@northumbria.ac.uk; Tel: +44 (0)191 227 3754

† Electronic supplementary information (ESI) available: The kinetic scheme and thermochemical data. See DOI: https://doi.org/10.1039/d4cy01205d

‡ Current address: Clean Air Ltd, Mill Street, Farnworth, Bolton, BL4 7BH, UK.

expressions are found by fitting the rate coefficients to match simulation results to one or several experiments and it is difficult to estimate the generality of the obtained expressions, the range of operating conditions and the types of catalysts to which they are applicable. The kinetic experiments are usually conducted in micro-reactors with characteristic dimensions of a few millimetres filled with powder catalysts, *e.g.* Chatterjee *et al.*[7] Arguably, the use of micro-reactors eliminates the influence of mass transfer from the gas phase to the catalyst surface. The temperature of the micro-reactor is homogeneous and tightly controlled, and flow rates through it are so small as to eliminate any spatial variation in gas and surface species concentrations. On the other hand, quantum chemistry simulations using either analytical forms of molecular orbitals, *e.g.* German and Sheintuch,[8] or density functional theory, *e.g.* Arnarson *et al.*,[9] are very useful in establishing the structure of possible transition states and the rate of associated reactions but owing to their heavy computational requirements, they are necessarily restricted to a limited number of configurations. Yet, together with available measurements, these methods allow one to clarify the mechanisms of the rate-limiting processes, that is conditions under which the overall rate of NO conversion is constrained by an elementary step of the chemical kinetics or physical kinetics, *e.g.* physisorption at or diffusion to the catalyst surface from the bulk of gas. Nonetheless, despite the progress achieved in studies of different factors in the selective catalytic reduction of nitric oxide by ammonia NH_3, see *e.g.* Kim *et al.*,[10] there does not seem to exist a comprehensive mathematical description of the latter including both physical and chemical rates of individual processes. Development of such a model is attempted here based on the generalised kinetics whereby the formulated kinetic pathways exploit the similarity of the redox cycles for the different types of catalysts and the rate constants for individual chemical reactions are estimated as average values across the range of catalysts. While this generalisation necessarily entails lower accuracy than the one attainable with fine tuning of the rates for a specific type of catalyst or SCR system design, it is worth emphasising that, owing to the complexity of the numerical modelling of flow and reactions in the SCR, a number of other assumptions are inevitable and the loss of accuracy caused by the use of generalised kinetics in simulations of a complete SCR system may well be smaller than that caused by other simplifications, *e.g.* the pattern of reducing agent spray entering the catalyst, *e.g.* if ammonia comes from decomposition of urea water solution as is commonly done in automotive applications.

The purpose of this work is thus to consider the generic elementary steps involved in NO reduction and estimate their rates from well-established dependencies. This is done with the hope that the resulting model, while perhaps not tuned to any particular type of catalyst, would nonetheless be capable of yielding an accuracy sufficient for an *a priori* analysis of a wide range of SCR exhaust aftertreatment systems through numerical simulations resolving simultaneously the gas flow and SCR chemistry. As shown by Jin *et al.*[11] a number of SCR catalysts have similar properties in terms of porosity, in the range 0.3…0.4, characteristic pore dimension, *circa* 10 nm, overall concentration of active sites, $0.5\ldots1.5 \times 10^{-3}$ mole cm^{-3}, and an attempt to utilise these similarities is made here through formulation of a generalised chemical kinetic mechanism and consideration of both physical and chemical steps in SCR processes.

2 Physical and chemical kinetics in SCR catalysts

The starting point in the development of this kinetic mechanism was the assumption that any catalytic site irrespective of its nature and composition may be attributed the same reaction rate constants. Though this assumption is obviously wrong as, *e.g.* it is well known that iron catalysts have much lower catalytic activity at lower temperatures compared to copper-exchanged zeolites or vanadia–tungsta catalysts, it proved nonetheless very useful in establishing the baseline kinetic mechanism, and estimating its rate constants. Departing from there, the difference in performance of different types of catalysts could then be reflected in changes of only a few rate constants while most of the scheme remains the same reflecting the generic features of SCR chemistry.

In what follows, Cat denotes the catalytic complex, *e.g.* Cu^{2+} in Cu – exchanged zeolites, or V^{5+} for vanadia catalysts, and Z denotes a substrate surface site capable of physisorption, *e.g.* SiOAl site for a zeolite or TiO_2 for a vanadia/tungsta catalyst. Charge changes are disregarded, that is Cat^- and Cat species are lumped together. Both surface and gaseous species are described in terms of their molar concentrations: this allows for a straightforward account of the surface coverage factor but makes it difficult to describe the neighbouring effects and the latter are neglected here. The differences between the activity of oligomeric, dimeric and polymeric active centres are reflected through introduction of several competing paths, the relative importance of which changes with temperature, catalyst loading and composition of the feed gas. Essentially, a given catalyst surface is imagined as a uniform substrate with a fixed molar surface density n_s of sites with a uniform fraction of oligomeric active sites.

This surface has a specific volumetric surface area identified here with the BET area; hence it is assumed that all reactions proceed either by the Eley–Rideal mechanism or in an adsorbed monolayer. It is assumed that, other than the catalytic sites, there are only 3 surface species: NH_3(s), NO_2(s) and O(s); the study of the role of the physiosorbed water and formation and reactions of surface hydroxyl are left for the subsequent work.

Two key catalytically active species in this mechanism are CatOH, designating the sites with Brønsted acidity, and CatO, a combination species with Lewis acidity. Together with the sites in an intermediate state they participate in a catalytic cycle shown in Fig. 1. The relative proportion of the CatOH and CatO sites existing in a degassed catalyst is an important characteristic of the latter: for vanadia-based catalysts with

virtually no Lewis acidity all active sites are taken as CatOH, while for metal-replaced zeolites the active sites are assumed to be mostly CatO. In order to make the model under development generic, *i.e.* applicable to variety of catalysts, it is proposed to combine mechanistically the pre-existing Lewis sites together with derivative CatO, *e.g.* produced by the sequence of reactions R1, R7 and R11 even though the valency of the catalyst metal would not be the same. This ansatz of lumping together catalyst sites with unequal valencies, hence possibly reactivity, is made solely to keep the model as simple as possible. It should be emphasised that both types of acidity refer to the catalyst sites and the effects of acidities on the substrate, see *e.g.* Ravi *et al.*,[12] are not considered: in this model the substrate itself is chemically passive but the three surface species adsorbed on it are reactive.

Fig. 1 depicts the summary of the proposed mechanism; in it, the main SCR loops are shown in blue solid lines, while the reactions pertinent to the so-called fast SCR loop involving NO_2 are shown as green dashed lines. Evacuation of the main reaction products, water vapour and nitrogen is not shown in order to simplify the diagram. It should be noticed that the reaction pathway involving the formation of nitrates at the catalytic site is represented here by reactions involving the CatONO complex; this aspect is further discussed below. As may be seen from Fig. 1, the proposed mechanism includes also the pathways for ammonia and NO oxidation at elevated temperatures, thus enabling simulations of effects of catalyst overheating. However, nitrous oxide N_2O and its reactions are excluded from the mechanism: it should be noticed that under most conditions, the yield of N_2O is very small at least in automotive applications. Competition between reactions involving NO and O_2 determines a progressive shift between different pathways of the redox cycle to ammonia oxidation at temperatures above 400 °C leading to worsening of NO conversion at more or less constant consumption of ammonia. The individual steps of the mechanism are considered in the subsequent sections.

In order to facilitate the inclusion of the proposed mechanism into the flow simulations, the rates of reactions and concentrations of both surface and gaseous species are expressed in this work as volumetric molar concentrations, following common convention for description of homogeneous reacting media. For a surface species Y, the volumetric concentration $[Y]$ is related to the coverage fraction Θ_Y and the surface concentration $\langle Y\rangle$ as:

$$[Y] = n_s \bar{S} \Theta_Y = \bar{S}\langle Y\rangle$$

where n_s is the total molar surface concentration and $\bar{S}$ is the BET surface area of the catalyst per unit volume. Here and in what follows the square and angle brackets denote specific quantities per unit volume and surface, respectively. In the estimations of the rate constants below, the value of n_s = 1.5 × 10^{-1} mole per cm^2 is taken as constant for all types of catalysts; this value corresponds to approximately 3 Å spacing between the molecules at the surface: for most SCR catalysts, the typical inter-site distance on the surface is $r_s \approx$ 2–3 Å. The BET area, *i.e.* catalyst specific surface area $\bar{S}$, an input parameter to this model, lies in the range of several tens to several hundred $m^2\ cm^{-3}$.

2.1 Adsorption of ammonia

There is ample experimental evidence that sorption of NH_3 may produce both strongly chemisorbed and weakly physiosorbed ammonia (Topsøe *et al.*,[4] Ma *et al.*,[13] and Hahn *et al.*)[14] The strong chemisorption of ammonia on a catalyst Brønsted acid site leads to the formation of bound ammonium, Han *et al.*:[1]

$$\mathrm{CatOH} + \mathrm{NH_3(g)} \underset{W_{1b}}{\overset{W_{1f}}{\rightleftarrows}} \mathrm{CatONH_4} \qquad \text{(R1)}$$

with a reverse process of desorption of NH_3 from the active site. This step is common for any catalyst site with Brønsted acidity, *e.g.* vanadia (Topsøe *et al.*,[4] Inomata *et al.*),[15] Nb–Cs (Ma *et al.*),[13] or Cu-exchanged zeolite (Janssens *et al.*)[3] Reaction of the Brønsted site with NO is ruled out owing to the evidence from experiments of Inomata *et al.*[15] and DFT simulations of Arnarson *et al.*[16] for vanadia catalysts with various dopants.

The rate W_{1f} of formation of ammonium bound on the catalytically active site, reaction R1, is determined by the ammonia diffusion from the gas phase proceeding with zero activation energy (Busca *et al.*),[17] with an accommodation steric factor ψ (sometimes also referred to as the "sticking coefficient") within the possible range of values 10^2–1 with the larger values for molecular adsorption:

$$W_{1f} = \psi F_{\mathrm{NH_3}} \langle S_{\mathrm{CatOH}}\rangle \qquad (1)$$

where $F_{\mathrm{NH_3}}$ is the molar flux of NH_3 from the bulk of the gas phase to the unit surface of the catalyst. The above expression incorporates the temperature T and pressure p dependency through the average thermal velocity $v_{\mathrm{NH_3}}$ and the molar density NH_3:

$$F_{\mathrm{NH_3}} = \frac{v_{\mathrm{NH_3}}}{6}[\mathrm{NH_3}] = \left(\frac{R_g T}{12 M_{\mathrm{NH_3}}}\right)^{1/2}[\mathrm{NH_3}] \qquad (2)$$

Here R_g is the universal gas constant, and $M_{\mathrm{NH_3}}$ is the molecular weight of ammonia. Eqn (2) assumes the equipartition of translational degrees of freedom. The specific surface area of the CatOH species $\langle S_{\mathrm{CatOH}}\rangle$ in eqn (1) is simply related to the CatOH concentration as:

$$\langle S_{\mathrm{CatOH}}\rangle = \Theta_{\mathrm{CatOH}}\bar{S} = \frac{[\mathrm{CatOH}]}{n_s} \qquad (3)$$

and, using the above expressions, the rate W_{1f} becomes:

$$\begin{aligned} W_{1f} &= \left(\frac{R_g T}{12 M_{\mathrm{NH_3}}}\right)^{1/2} n_s^{-1} \psi_{1f} [\mathrm{NH_3}][\mathrm{CatOH}] \\ &= \psi_{1f} k_{1f} [\mathrm{NH_3}][\mathrm{CatOH}] \end{aligned} \qquad (4)$$

where the "pseudo-pre-exponential factor", k_{1f}, may be estimated as $k_{1f} \approx 4 \times 10^{11}\ T^{0.5}$ ($k_{1f} \approx 10^{13}$ cm^3 per mole s at T =

600 K); the accommodation steric factor, or "sticking probability", ψ_{1f} is taken here as one, a common value for molecular adsorption (Zhdanov).[18]

Because k_{1f} is effectively the rate of collisions of gas molecules with a unit surface, in what follows its value will be used as the upper limit for the pre-exponential factor of other reactions involving gaseous species. Zero activation energy and ψ in the range 0.1–1 are common for molecular adsorption on active catalyst sites, Zhdanov.[18]

For a typical SCR catalyst, Θ_{CatOH}, the surface fraction of the Brønsted acid sites, lies in the range from 0.01, (or, obviously, even 0 for catalysts which do not exhibit protonation, *e.g.* Lietti *et al.*[19]) to a rather extreme value of Θ_{CatOH} = 0.6, Alemany *et al.*,[20] with typical values for most industrial catalysts of 0.02–0.04; thus [CatOH] ranges from 10^{-4} to 10^{-3} mole per cm^3. With the values in the middle of this range, eqn (4) yields the inverse characteristic time of NH_3 adsorption k_{1f}[CatOH] $\approx 3 \times 10^9$ s^{-1}. It is worth noticing that, though eqn (2) and (4) use expressions for thermal velocity in the bulk gas phase, the characteristic time of adsorption so obtained is very close to that of gaseous diffusion over a distance, *e.g.* pore diameter, of $r_p = 2 \times 10^{-6}$ cm:

$$\frac{\Theta_{\mathrm{CatOH}} D_{\mathrm{NH_3}}}{{r_p}^2} \approx 4 \times 10^9\ \mathrm{s}^{-1} \tag{5}$$

It should also be mentioned that the above estimation of the inverse characteristic time is well within the range recommended by Zhdanov[18] but much larger than the values in the range of 10^3–10^4 s^{-1} used previously in some applied simulations, *e.g.* Chatterjee *et al.*,[7,21] Schmeisser *et al.*[22]

Reverse reaction to (R1) is the desorption of strongly bound NH_3 from the active site, the characteristic time of which is

$$\tau_{\mathrm{des}} = k_{1b}^{1} \exp\left(\frac{E_{1b}}{R_g T}\right) \tag{6}$$

where the pre-exponential factor for desorption k_{des} may be estimated using analysis of Campbell *et al.*[23] involving the difference of entropies S of the adsorbed NH_3(s) and gaseous NH_3 species:

$$\begin{aligned} k_{1b} &= \frac{k_B T}{h} \exp\left(\frac{S_{\mathrm{NH_3(g)}} - S_{\mathrm{NH_3(s)}}}{R_g}\right) \\ &\approx \frac{k_B T}{h} \exp\left(0.33 + \frac{0.3 S_{\mathrm{NH_3(g)}} - S^{1Dtrans}_{\mathrm{NH_3(g)}}}{R_g}\right) \end{aligned} \tag{7}$$

where k_B and h are Boltzmann and Planck constants, respectively, $\left(\frac{k_B T}{h} \approx 2.6 \times 10^{12}\ T\ \mathrm{s}^{-1}\right)$. The entropy $S^{1Dtrans}_{\mathrm{NH_3(g)}}$ of gaseous ammonia with one translational degree of freedom removed may be estimated Campbell *et al.*[23] at T_0 = 298 K using the standard entropy of formation of argon S^0_{AR} as:

$$S^{1Dtrans}_{\mathrm{NH_3(g)}} = \frac{1}{3}\left(S^0_{\mathrm{Ar}} + R \ln\left[\left(\frac{M_{\mathrm{NH_3}}}{M_{\mathrm{Ar}}}\right)^{\frac{3}{2}}\left(\frac{T}{T_0}\right)^{\frac{5}{2}}\right]\right) \tag{8}$$

where the $M_{\mathrm{NH_3}}$ and M_{Ar} are the molecular weights of ammonia and argon, respectively. Using the tabulated values Vargaftik[24] of $S^0_{\mathrm{AR}} = 18.6 R_g$, $S_{\mathrm{NH_3}}(400\ \mathrm{K}) = 205$ J mole^{-1} K^{-1}, one may obtain that the pre-factor in eqn (7) at T = 400 K, $k_{1b} \approx 8.4 \times 10^{14}$ s^{-1} increasing to $k_{1b} \approx 1.6 \times 10^{15}$ s^{-1} at 600 K. This estimation does not depend on the nature of the sorbent.

The activation energy for desorption of NH_3 strongly adsorbed on the Brønsted sites was derived from temperature-programmed desorption experiments in Colombo *et al.*[25] as $E_{1b} \approx$ 106–116 kJ per mole. Using these values in eqn (6), one obtains at 400 K the characteristic time for desorption $\tau_{\mathrm{des}} \approx 0.28$ s, *i.e.* about eight orders of magnitude larger than the characteristic time for adsorption owing to the large activation energy of desorption. For different types of zeolites and silica–alumina catalysts with significant concentration of the acid cites, fairly wide distributions of the desorption activation energy were measured in Masuda *et al.*[26] with maximum probabilities in the range of 70–110 kJ per mole. Thus, in the lower range of temperatures typical for SCR operation, the equilibrium of reaction R1 is strongly shifted to absorption on active sites.

An alternative path of $CatONH_4$ formation is through the Langmuir–Hinshelwood mechanism, *i.e.* weak physisorption of NH_3 on the metal oxide sites of the substrate Z with subsequent surface diffusion to and chemisorption at an active site:

$$\mathrm{NH_3(g)} + Z \underset{W_{2b}}{\overset{W_{2f}}{\rightleftarrows}} \mathrm{NH_3(s)} \tag{R2}$$

$$\mathrm{CatOH} + \mathrm{NH_3(s)} \overset{W_3}{\rightarrow} \mathrm{CatONH_4} \tag{R3}$$

Strictly speaking, the rates of these processes depend on the nature of the substrate and the structure of the surface. Even though it has been shown that for some catalysts, *e.g.* V/W/TiO_2, NH_3 sorption on TiO_2 is molecular with the accommodation factor ψ_2 in the range 0.2–0.4, Diebold and Madey,[27] in the presence of oxygen or surface hydroxyl radicals from dissociatively adsorbed water vapour, chemisorption may not be excluded, see *e.g.* Dastoor *et al.*[28] Following the arguments for the rate of adsorption on the active sites, the rate of physisorption on the substrate per unit catalyst volume may be estimated as

$$W_{2f} = \psi_2 k_{1f} [\mathrm{NH_3}][Z] \tag{9}$$

proceeding with zero activation energy and $\psi_2 \approx 0.25$. The concentration of Z is $[Z] = \Theta_Z n_s \bar{S}$ where Θ_Z is the ratio of surface sites capable of physisorption to the total surface molecular concentration, *e.g.* Θ_Z = 1 for the tungsta substrate and for SSZ zeolites Θ_Z may be taken as equal to the Al/Si molar ratio.

The rate of desorption of weakly sorbed NH_3(s) is

$$W_{2b} = k_{2b} \exp\left(-\frac{E_{\mathrm{des}}}{R_g T}\right)[\mathrm{NH_3(s)}] \tag{10}$$

The pre-exponential factor in the above equation may be estimated using the same procedure involving the difference in entropies: $k_{2b} \approx 2.6 \times 10^{12}$ T [s^{-1}] in the temperature range

relevant for SCR operation. Modelling of Colombo *et al.*[25] used the activation energy E_{des} = 46.5 kJ per mole for the desorption of weakly adsorbed NH_3 for Fe-activated zeolite. However, using synchrotron PXRD experiments Ye *et al.*[29] showed for H-ZSM-5 zeolite a distribution of the desorption energies with peaks at 7, 21 and 113 kJ per mole corresponding to activation barriers for very weak interactions, N–H⋯O, hydrogen bonding N–H⋯N, and strong Brønsted acid–base adduct formation O⋯+HN, respectively. Here it is assumed that the adsorption on the substrate is through the formation of hydrogen bonds only, thus the desorption activation energy is taken as $E_{2\mathrm{b}}$ = 42 kJ per mole: the chemisorption is considered only on the catalytically active sites but not on the substrate. The reason for this is that, while adsorption of water always present in the exhaust is likely to increase the prominence of NH_3 sorption through hydrogen bonding, co-adsorption of water and ammonia on passive surfaces is beyond the scope of the present work.

Taking into account that the amount of the available sorption sites $[Z]$ remains approximately constant, as it is verified below, the ratio of concentrations of physiosorbed and gaseous ammonia may be found if reaction R2 is in partial equilibrium:

$$\frac{[\mathrm{NH_3(s)}]}{[\mathrm{NH_3}]} = \frac{\psi_2 k_{1f} \Theta_Z n_s \bar{S}}{k_{\mathrm{des}} \exp\left(-\frac{E_{\mathrm{des}}}{R_g T}\right)} \tag{11}$$

This ratio may be estimated at 400 K at 6×10^{-4} with temperature rise decreasing this ratio further still. Work of Campbell *et al.*[23] showed that the pre-exponential $k_{1\mathrm{b}}$ has only a weak, within one order of magnitude, dependency on the adsorbate structure or composition, however, the issue of chemisorption of NH_3 on hydroxyl layers in the presence of water vapour in the gas, *e.g.* forming the O^*HNH_3 complex in the substrate, would deserve a further study.

Formation of $CatONH_4$ from the weakly adsorbed ammonia proceeds through surface diffusion of the ammonia to a much heavier, hence less mobile, catalytic site, followed by reaction R3. The characteristic time for the surface diffusion is $\tau_{\mathrm{d}} \approx \frac{d_{\mathrm{c}}^2}{4D}$ where d_{c} is an average distance between two catalyst sites, $d_{\mathrm{c}} \sim (\Theta_{\mathrm{CatOH}} n_s N_A)^{-1/2}$ and D is the surface diffusivity. The activation energy for surface diffusion is low, Zhdanov,[18] and, assuming a typical value of $D \approx 10^{-3}$ $\mathrm{cm^2\ s^{-1}}$,[30] one may estimate $\tau_{\mathrm{d}} \approx 1.4 \times 10^{-12}$ $\mathrm{s^{-1}}$. Therefore, the rate of reaction R3 between two surface species:

$$W_3 = k_3 \exp\left(\frac{E_3}{R_g T}\right)[\mathrm{NH_3(s)}][\mathrm{CatOH}] \tag{12}$$

may be assumed to proceed with very low activation energy $E_3 \approx 0$, Chorkendorff and Niemanrsverdriet,[30] and its pre-exponential factor k_3 may be estimated as follows.

As reaction R3 is an addition, its activated complex is the same as the final product, and its formation comes with loss of two translational and one rotational degree of freedom (DOF) of NH_3(s). For one translational DOF of a physiosorbed molecule, the partition function $q_{\mathrm{T}} = \frac{d}{\Lambda}$ where the cell size d is essentially the distance between two sorption sites, $d \approx r_s$:

$$d \approx (\Theta_Z n_s N_A)^{1/2} \approx (1.5 \times 10^{-9}\ \mathrm{mole\ cm^{-2}} \times 6.02 \times 10^{23}\ 1/\mathrm{mole})^{-1/2} \approx 2 \times 10^{-8}\ \mathrm{cm}$$

and the thermal wavelength at 400 K

$$\Lambda = \frac{h N_A^{1/2}}{(2\pi M_{\mathrm{NH_3}} kT)^{1/2}} \approx 2 \times 10^{-9}\ \mathrm{cm}$$

Thus, one translational DOF partition function q_{T} = 15. For one rotational DOF the partition function q_{R} may be estimated as

$$q_{\mathrm{R}} \approx \frac{T^{1/2}}{(\Pi_1 \Pi_2 \Pi_3)^{1/6}}$$

with the rotational temperatures $\Pi_{1,2,3}$ = 13.6, 13.6, and 8.9 K for ammonia. Thus at 400 K $q_{\mathrm{R}} \approx 7$. Then the characteristic reaction time τ_3 for reaction R3 may be found as

$$\tau_3 = \frac{h q_{\mathrm{T}}^2 q_{\mathrm{R}}}{kT} \approx 2 \times 10^{-10}\ \mathrm{s} \tag{13}$$

This time is much, by about two orders of magnitude, larger than the surface diffusion time τ_{d} found above, therefore the chemical transformation is the limiting stage defining the pre-exponential factor k_3. When the rate of a bimolecular reaction is written for the molar concentrations of surface species its pre-exponential factor becomes:

$$k_3 = \frac{1}{\tau_3 n_s \bar{S}} \approx 2 \times 10^{12} \frac{\mathrm{cm^3}}{\mathrm{mole\ s}} \tag{14}$$

It is worth mentioning that the above value is about one order of magnitude larger that the values that may be derived from the recommendations of Zhdanov[18] for the frequency ν of the bimolecular reaction between the adsorbed species, $\nu = 10^{13}$–10^{14} $\mathrm{s^{-1}}$. One may also see that the reaction R3 is much faster than ammonia desorption, especially for a lower range of SCR operation temperatures. Taking into account fast surface diffusion and relatively fast reaction time, as well as the low equilibrium ratio of physiosorbed ammonia concentration to that of gaseous NH_3, one may see why the weakly adsorbed ammonia is commonly not detected in experiments, see *e.g.* Inomata *et al.*:[15] effectively, reaction R3 acts as a fast sink for relatively small amounts of physiosorbed NH_3(s).

In formulation of the proposed mechanism it is assumed that both gaseous and physiosorbed ammonia adducts molecularly on Lewis acid cites: this assumption is supported by the spectroscopic observations of Suárez *et al.*[31] This assumption leads to the following reactions:

$$\mathrm{CatO} + \mathrm{NH_3(g)} \xrightarrow{W_4} \mathrm{CatONH_3} \tag{R4}$$

$$\mathrm{CatO} + \mathrm{NH_3(s)} \xrightarrow{W_5} \mathrm{CatONH_3} \tag{R5}$$

As a matter of fact, chemisorption of NH_3 on CatO and formation of $CatONH_3$ through a valent bond involves electron transfer from NH_3 and is therefore equivalent to an action of a Lewis acid cite, except that in this case CatO may also be a derivative site formed as a part of the catalytic cycle. A number of novel catalysts, however, do not exhibit Brønsted acidity at all, Jin *et al.*,[11] Han *et al.*,[1] and for those reaction R4 should be taken as the departure point for description of the SCR redox cycles.

As shown in Arnarson *et al.*,[9] reaction R4 has a relatively low activation energy of E_3 = 7.4 kcal per mole for reduced CatO while pre-existing, *i.e.* non-reduced Lewis sites should chemisorb NH_3(g) with an activation barrier greater than or at least equal to E_3 and a much smaller accommodation factor, Yin *et al.*[32] However, doping catalysts, *e.g.* vanadia with CeO_2, accelerates chemisorption, Han *et al.*,[1] thus increasing the accommodation factor and lowering the activation energy. Hence, the rate constants for reaction R4 may be estimated as $\psi_4 k_{1f}$ with lowered ψ_4 = 0.3 to account for asymmetry of NO and E_3 = 30 kJ per mole. The low value of the activation energy for the adsorption at the Lewis site is also in agreement with Marberger *et al.*,[33] see also ref. 6 therein.

Reaction R5 is a bimolecular association of two surface species, thus for it one may safely assume zero activation energy and the characteristic frequency factor of 10^{14} s^{-1}, Zhdanov,[18] corresponding to the pre-exponential factor of $k_r \approx 5\times10^{15}\frac{cm^3}{mole\ s}$. On the other hand, the pre-exponential factor for the surface diffusion $k_d \approx (\tau_d n_s \bar{S})^{-1}$ may be estimated as $4\times10^{12}\frac{cm^3}{mole\ s}$, thus this reaction is diffusion-controlled, non-activated and $k_5 = k_d$.

2.1.1 Redox cycles. The envisaged normal SCR cycle comprises two steps of NO reduction and one step of oxidation with O_2 in order to satisfy the overall stoichiometry. Reactions with NO or oxygen proceed in parallel for most states of the catalytic site, starting with the complex $CatONH_4$ formed in reactions R1 and R3, see Fig. 1. The reaction of the complex $CatONH_4$ with gaseous NO forms gaseous water, nitrogen, and a reduced active catalyst site:

$$CatONH_4 + NO \xrightarrow{W_6} Cat + N_2 + 2H_2O \qquad (R6)$$

This reaction has been very extensively studied, see *e.g.* Arnarson *et al.*[9] It may be thought as a succession of several steps: diffusion of NO with formation of an activated complex and consequent split of the latter, and evacuation, either by the surface diffusion or desorption of H_2O, N_2, and H_2O again: *a priori* any of these steps may be rate limiting under a particular set of conditions.

The overall rate of reaction R6 may therefore be represented as:

$$W_4 = \left(W_{NO}^{-1} + 2W_{sH_2O}^{-1} + 2W_{eH_2O}^{-1} + W_{sN_2}^{-1} + W_{eN_2}^{-1}\right)^{-1} \qquad (15)$$

where W_{NO} is the rate of formation of the transition state $CatONH_4NO$, W_{sH_2O} and W_{eH_2O} are the rates of water scission and removal from the site, *i.e.* desorption and surface diffusion, W_{sN_2} and W_{eN_2} are the rate of molecular nitrogen scission and removal, respectively. The rates of these individual steps may be estimated as follows.

Results of DFT simulations by Arnarson *et al.*[9] show that formation of the transition state proceeds with activation energy E_{NO} of 13.6 kcal per mole. Invoking a usual Arrhenius expression for its rate:

$$W_{NO} = k_{NO}\exp\left(-\frac{E_{NO}}{R_g T}\right)[NO][CatONH_4] \qquad (16)$$

the pre-exponential factor k_{NO} should be determined by the rate of flow of NO from the gas phase. Similar to the previous derivation for NH_3, k_{NO} may be written as

$$k_{NO} = \psi_{NO} k_{1f}\left(\frac{M_{NH_3}}{M_{NO}}\right)^{1/2}$$

While data on the accommodation factor ψ_{NO} are not available and its precise value depends on the nature of the catalyst, it may be tentatively estimated as $\psi_{NO} \approx 005$, the value in the range between the ranges for molecular and associative adsorption. Thus $k_{NO} = 1.5\times10^{11}\ T^{1/2}\frac{cm^3}{mole\ s}$ yielding the characteristic time of this reaction of order of 0.2 s for typical NO molar densities in an exhaust gas at 600 K.

Scission of both water and nitrogen occurs with zero activation energy, and does not activate any additional degrees of freedom in the transition state, hence their pre-exponent factors are those of the monomolecular reaction of an adsorbed species, for which a typical value (Zhdanov)[18] is $k_S = \frac{kT}{h}$, *e.g.* at T = 500 K $k_{sH_2O} = k_{sN_2} = 10^{13}$ s^{-1}, hence

$$W_{sH_2O} = W_{sN_2} = k_s[CatONH_4NO] \qquad (17)$$

It is obvious that the scission step is much faster than the formation of the activated complex $CatONH_4NO$ at any temperature, hence it cannot be rate limiting.

The rate of removal of products, *e.g.* water, away from the active site, is the sum of the rates of desorption W_{desH_2O} from the active site and the surface diffusion, W_{diffH_2O} away from the site:

$$W_{eH_2O} = W_{diffH_2O} + W_{desH_2O} \qquad (18)$$

The pre-exponential factors for the desorption are determined following the same procedure of Campbell *et al.*[23] invoking entropy differences at 400 K and 600 K as:

$$k_{desH_2O}(400K) = 7.0\times10^{14}\ s^{-1} \quad k_{desH_2O}(600K) = 1.3\times10^{15}\ s^{-1}$$

$$k_{desN_2}(400K) = 5.9\times10^{14}\ s^{-1} \quad k_{desN_2}(600K) = 9.7\times10^{14}\ s^{-1}$$

The activation energy for the desorption from the active site is estimated here from the measurements of the rate of

desorption extrapolated to unity coverage, $\Theta = 1$. For N_2 the experiments of Scholten *et al.*[34] on desorption from iron films yield $E_{\mathrm{desN_2}}(\Theta) = 55.0 - 29.2\Theta$[kcal per mole] with the value extrapolated to full coverage $E_{\mathrm{desN_2}} = 25.8$ kcal per mole; this value is adopted here as an average for different substrates owing to the lack of data for other types of catalyst substrates. For the desorption of water, the activation energy reported for zeolites in Fan *et al.*[35] changed from approximately 20 kcal per mole at lower temperatures, 300–450 K, to just above 70 kcal per mole at 600–700 K; the reported value also depended, albeit with a smaller variation, upon the zeolite structure and what alkali metal, Li or Na, cations were used for charge compensation. The average value, measured in Fan *et al.*[35] at temperatures of 500–600 K, of $E_{\mathrm{desH_2O}} \approx 40$ kcal per mole, was about twice larger than the value of 18 kcal per mole reported for different TiO_2 crystals in Henderson.[36] Close to the latter, values of approximately 15 kcal per mole were reported for different types of zeolites in Prokof'ev *et al.*[37] and similar figures of 16.6 kcal per mole for silica in Feng *et al.*[38] For the overall rate estimations, the value of $E_{\mathrm{desH_2O}} = 20$ kcal per mole is retained here.

Compared to desorption, the surface diffusion has very low activation energy which may safely be assumed as zero, and its rate constants may be estimated as, Campbell *et al.*:[23]

$$k_{\mathrm{diff}} = \frac{k_B T}{h} \exp\left(-\frac{S^{1Dtrans}}{R_g}\right) \tag{19}$$

leading to:

$$k_{\mathrm{diffH_2O}}(400\mathrm{K}) = 2.0 \times 10^{10}\ \mathrm{s}^{-1} \quad k_{\mathrm{desH_2O}}(600\mathrm{K}) = 1.4 \times 10^{10}\ \mathrm{s}^{-1}$$

$$k_{\mathrm{desN_2}}(400\mathrm{K}) = 1.6 \times 10^{10}\ \mathrm{s}^{-1} \quad k_{\mathrm{desN_2}}(600\mathrm{K}) = 1.1 \times 10^{10}\ \mathrm{s}^{-1}$$

Comparing these values with the rates of desorption, one may see that for nitrogen the surface diffusion is faster than the desorption over the entire range of temperatures relevant to SCR operation (300–1000 K) and in the range of 300–900 K for water. Moreover, one may also see that the product removal is many orders of magnitude faster than the chemisorption reaction R6, hence, to a very good approximation the overall rate is given by the limiting step eqn (16).

Reaction R6 or one of its variations features in every kinetic scheme of SCR operation, meanwhile reactions of ammonium bound on a catalytic site with molecular gaseous oxygen are, with notable exceptions of Arnarson *et al.*[9] and Cheng *et al.*,[39] invariably absent from consideration. This is rather surprising as a typical exhaust gas contains at least ten times more O_2 than NO. In order to clarify the pathways of reactions involving oxygen, consider the following reaction, a partial oxidation of bound ammonium:

$$\mathrm{CatONH_4} + \mathrm{O_2} \xrightarrow{W_7} \mathrm{CatONH_2} + \mathrm{O(s)} + \mathrm{H_2O} \tag{R7}$$

producing physiosorbed atomic oxygen O(s). The above reaction is a very much simplified but stoichiometrically correct representation of several elementary steps analysed in Arnarson *et al.*,[9] it may be inferred from their analysis that this reaction R7 proceeds with the overall activation energy of $E_7 = 215$ kcal per mole. Its pre-exponential factor, determined by the flux of gaseous O_2, may be estimated in the same manner as it was done for reactions R2 and R6: $k_7 = \psi_7 k_{1f}\left(\frac{M_{\mathrm{NH_3}}}{M_{\mathrm{O_2}}}\right)^{1/2}$ with the accommodation factor $\psi_7 \approx 1$. Owing to its larger activation energy, this reaction is about four orders of magnitude slower than reaction R6 at low temperatures, but with the rise of temperature the difference progressively decreases so that at approximately 950 K both reactions proceed at the same rate. Following the same method as for reaction R6, it may be shown that neither scission nor evacuation of the products is the rate-limiting step.

In principle, the same rate constants as for reaction R7 may also be ascribed to other reactions consuming gaseous oxygen, *e.g.* oxidation of the reduced active site Cat formed in reaction R6:

$$\mathrm{Cat} + \mathrm{O_2} \xrightarrow{W_8} \mathrm{CatO} + \mathrm{O(s)} \tag{R8}$$

or further steps in oxidation of bound ammonium following reaction R7:

$$\mathrm{CatONH_2} + \mathrm{O_2} \xrightarrow{W_9} \mathrm{CatONO} + \mathrm{H_2O} \tag{R9}$$

$$\mathrm{CatONH_2} + \mathrm{O_2} \xrightarrow{W_{10}} \mathrm{CatO} + \mathrm{NO} + \mathrm{H_2O} \tag{R10}$$

with the sum of the accommodation factors for the latter two reactions equal to or less than one so that their summary pre-exponential does not exceed the gaseous oxygen diffusive flux, hence values $\psi_9 = \psi_{10} = 0.5$ are taken here. The above three reactions describe two alternative oxidation pathways and, in order to distinguish low-temperature and high-temperature branches, reaction R8 is ascribed the activation energy of E_8 of 80 kJ per mole, a value lower than E_7 while the activation energies for reactions R9 and R10 are taken larger than E_7, at $E_9 = E_{10} = 125$ kJ per mole.

In parallel with the above oxidation reactions, $CatONH_2$ also reduces NO as:

$$\mathrm{CatONH_2} + \mathrm{NO} \xrightarrow{W_{11}} \mathrm{CatOH} + \mathrm{N_2} + \mathrm{H_2O} \tag{R11}$$

with the activation energy equal or somewhat smaller than that of reaction R6; owing to the lack of other data, the same rate constants are taken for this reaction as for reaction R6.

The cycle of active site transformations envisaged so far to represent the so-called normal SCR operation may now be closed with the following two reactions returning the active site its Brønsted acidity:

$$\mathrm{CatONH_3} + \mathrm{NO} \xrightarrow{W_{12}} \mathrm{CatOH} + \mathrm{N_2} + \mathrm{H_2O} \tag{R12}$$

$$\mathrm{CatONH_3} + \mathrm{O_2} \xrightarrow{W_{13}} \mathrm{CatOH} + \mathrm{NO} + \mathrm{H_2O} \tag{R13}$$

It has been noticed that, compared with Brønsted sites, the Lewis sites have higher reactivity. As the pre-exponential factors for the two above reactions are determined by the rate of diffusion of NO and O_2 from the gas phase, both proportional to k_{1f}, and they are likely to have only a small difference in the accommodation factors, the latter may be taken essentially equal to those for reactions R6 and R7. The higher reactivity of the $CatONH_3$ state may thus only be reflected through the activation energies for the above two reactions being lower than those of the counterpart reactions with $CatONH_4$. As a first approximation, the activation energy for reaction of $CatONH_3$ with oxygen is taken the same as for $CatONH_4$ as E_{13} = 21.4 kcal per mole but reduced by 20% for reaction with NO, $E_{12} \approx 11$ kcal per mole.

While reactions R12 and R13 complete the normal SCR cycle ensuring correct stoichiometry, there is a significant body of evidence, *e.g.* Nova *et al.*,[40] Ma *et al.*[41] that oxidation of active sites proceeds through formation of nitrates, *e.g.* $CatONH_4NO_3$ and a set of reactions with overall stoichiometry of $CatNO_3 + NH_4 \rightarrow CatO + 2H_2O + N_2$. Furthermore, the presence of NO_2 in exhaust gas, as *e.g.* may be formed in diesel engines at the cold start and at low loads, may lead to the SCR cycle proceeding in the so-called "fast SCR" mode with different stoichiometry, Koebel *et al.*,[42] Leistner *et al.*[43] It should be noticed that taking into account the surface atomic oxygen species O(s) means that, even if there is no nitrogen dioxide in the exhaust, it could be produced through direct reaction NO(g) + O(s) → NO_2 introduced later as reaction R16, hence, NO_2 kinetic pathways should be taken into account too. Increased SCR activity at low temperatures favouring adsorption over desorption suggests that sorbed NO_2(s) species should be considered alongside gaseous NO_2(g), and this is considered in the next section.

The rates of reactions of oxidation by physiosorbed atomic oxygen and another surface species, *e.g.*:

$$CatONH_4 + O(s) \overset{W_{14}}{\rightarrow} CatONH_2 + H_2O \quad (R14)$$

$$Cat + O(s) \overset{W_{15}}{\rightarrow} CatO \quad (R15)$$

are determined by the surface diffusion of O(s) as the active catalytic species are much less mobile owing to their larger molecular mass. The pre-exponential factor for the above reactions is of the order $k_{11} = k_{12} \approx 5 \times 10^{12}$ cm^3 per mole per s, and these reactions proceed with zero activation energy owing to the high reactivity of the atomic oxygen. It is interesting to notice that, at least in principle, a switch of the reduction cycle to the so-called fast SCR loop involving NO_2 may be initiated by the following surface reaction proceeding on a substrate, even if there is no nitrogen dioxide originally in the exhaust:

$$O(s) + NO \overset{W_{16}}{\rightarrow} NO_2(s) \quad (R16)$$

The rate of reaction R16 is determined by the NO diffusion from the gas phase, thus $k_{16} \approx k_{1f}\left(\frac{M_{NH_3}}{M_{NO}}\right)^{1/2}$ with unity accommodation factor and zero activation energy.

2.2 NO_2 pathway and fast SCR

The usual interpretation of the so-called "fast SCR" cycle is that it involves gaseous nitrogen dioxide NO_2 in concentration comparable to that of NO.[42,43] While combustion in modern either spark or compression ignition engines does not commonly produce NO_2 in any significant amounts, it may be expected that for certain operating conditions it could be formed in the exhaust circuit from NO through gas phase reactions with oxygen or water vapour. The mechanism of NO_2 formation in the gas phase is beyond the scope of this work, nonetheless, assuming that NO_2 is present in the exhaust, the previous investigations of the fast SCR mechanism, see *e.g.* Arnarson *et al.*,[9] highlight the CatONO complex as the principal surface intermediate. Consideration of this complex and its pathways in this model also represents reactions involving well-documented nitrate species, *e.g.* Ma *et al.*,[41] involved as intermediates in the SCR cycle.

Other than reaction R9, CatONO may be formed in reactions involving both gaseous and surface species:

$$CatO + NO \underset{W_{17b}}{\overset{W_{17f}}{\rightleftarrows}} CatONO \quad (R17)$$

$$Cat + NO_2(g) \underset{W_{18b}}{\overset{W_{18f}}{\rightleftarrows}} CatONO \quad (R18)$$

$$Cat + NO_2(g) \overset{W_{19}}{\rightarrow} CatONO \quad (R19)$$

According to the meaning of CatO as Lewis acid sites adopted in this model, reaction R17 means chemisorption of NO on an active site, hence, the desorption should also be considered for consistency with analysis of reaction R1. Weak NO adsorption on the substrate is not considered following the findings of Lietti *et al.*[19] and Sivachandiran *et al.*[44]

The desorption activation energies E_{17b} and E_{18b} depend on the type of catalyst and, arguably, the substrate and composition of the exhaust gas; using a single value for either in this model is, by necessity, a compromise aiming at applicability to several catalyst types. Adsorption and desorption of NO were studied quite extensively, in particular in relation to the oxidation on platinum catalysts, *e.g.* Ghosh *et al.*,[45] Crocoll *et al.*,[46] and storage in absorbers, *e.g.* Villamaina *et al.*,[47] Ambast *et al.*[48] It was found that increase of water vapour or carbon monoxide coverage fraction of the catalyst inhibits the desorption while oxygen promotes it. For example, for dry and oxygen saturated Pt catalysts, desorption activation energies of 114 and 104 kJ per mole, respectively, were reported by Crocoll *et al.*[46] At the same time, experiments of Lietti *et al.*[19] reported virtually no adsorption of NO in vanadia catalysts thus indicating a very small desorption activation energy and a strong shift of equilibrium in reaction R17 to the left. Work of Wentworth *et al.*[49] quoted the range of 90–140 kJ per mole and, accepting temperature as a proxy for the coverage fraction, proposed an expression for desorption activation energy decreasing from 105 to approximately 75 kJ per mole over the range of temperatures

encountered in an automotive SCR. Very strong suppression of NO adsorption by water vapour was noticed by Despres *et al.*[50] Adsorption of NO in Cu-exchanged zeolites proceeds through formation of copper mono- or dinitrosyls with the bond energies dependent on the zeolite structure and coordination of the N–O bonds: clearly, no single value may be attributed to the diverse cases. A binding energy of 22 kcal per mole average over different configurations is reported by Treesukol *et al.*[51] for Cu-exchanged ZSM5 zeolite. Therefore, a compromise value of E_{17b} of 78 kJ per mole is adopted here from pragmatic considerations that this value should describe the equilibrium shift in reaction R17 from strong absorption at low temperatures to nearly complete desorption at higher temperatures of typical automotive SCR conditions.

If one defines the equilibrium constant for reaction R17 as

$$K_{\mathrm{des}} = \frac{[\mathrm{CatONO}]}{[\mathrm{NO}][\mathrm{CatO}]} = \frac{\psi_{17f} k_{17f}}{k_{17b}} \exp\left(\frac{E_{17b}}{R_g T}\right) \tag{20}$$

and takes into account that fugacity coefficients for the surface species are very close to one, one may see that a nearly complete desorption means $K_{\mathrm{des}} \approx [\mathrm{NO}]_0^1$ where the typical NO concentration in the exhaust gas is $[\mathrm{NO}]_0 \sim 10^{-8}$ mole per cm^3. Estimating the pre-exponential factors as $\psi_{17f} k_{17f} = 3 \times 10^{11}\ T^{1/2}$ cm^3 per mole per s and $k_{17b} = 2 \times 10^{13}$ 1 s^{-1} (Baetzold and Somorjai),[52] and assuming that at 500 K there is no appreciable adsorption, one may obtain $E_{17b} = 78$ kJ per mole. This value is about 20% less than the 105 kJ per mole calculated with *ab initio* methods in Zhanpeisov *et al.*[53] for Cu+ model zeolites, but very close to the values obtained in Treesukol *et al.*[51] and experiments discussed therein.

Strong chemisorption of NO_2 on Cu–β zeolite was noticed in Wilken *et al.*[54] The reversible reaction R18 describes chemisorption and desorption of gaseous NO_2 on a modified active site; thus, its forward step is non-activated and the activation energy for the reverse step is the same as the heat of NO_2 adsorption, reported as 65 kJ per mole for Cu–β zeolite in Wilken *et al.*[54] The pre-exponential factors may be estimated as $\psi_{18f} k_{18f} = 1.5 \times 10^{10}\ T^{1/2}$ cm^3 per mole per s and $k_{18b} = 2 \times 10^{13}$ 1 s^{-1}. Accepting these values and the results of experiments of Sivachandiran *et al.*[44] showing that most (97%) NO_2 is strongly absorbed on tungsta with a desorption temperature of about 580 K leads to the value of $E_{18b} = 120$ kJ per mole and this value is adopted here. The rate of bimolecular association, reaction R19, is determined by the non-activated surface diffusion of NO_2(s), $k_{19} \approx 3 \times 10^{12}$ cm^3 per mole per s, $E_{19} = 0$.

Reactions with either gaseous or physiosorbed ammonia transform the complex CatONO representing nitrates back to the Brønsted acid site CatOH, the departure point for the redox cycles envisaged here:

$$\mathrm{CatONO} + \mathrm{NH_3} \overset{W_{20}}{\rightarrow} \mathrm{CatOH} + \mathrm{N_2} + \mathrm{H_2O} \tag{R20}$$

$$\mathrm{CatONO} + \mathrm{NH_3(s)} \overset{W_{21}}{\rightarrow} \mathrm{CatOH} + \mathrm{N_2} + \mathrm{H_2O} \tag{R21}$$

As follows from the DFT simulations of Arnarson *et al.*,[9] reaction R20 should have an activation barrier, $E_{F20} = 7.9$ kcal per mole and its pre-exponential factor is the same as of reaction R1. The pre-exponential factor of the non-activated reaction R21 is determined by the surface diffusion of NH_3(s), $k_{21} \approx 4 \times 10^{12}$ cm^3 per mole per s.

Nitrogen dioxide is involved in the fast SCR cycle and reactions of oxidation of nitric oxide and ammonia. Within the postulated set of species, the following reactions may be envisaged for the fast SCR cycle, see the green lines in Fig. 1:

$$\mathrm{CatONH_4} + \mathrm{NO_2(g)} \overset{W_{22}}{\rightarrow} \mathrm{CatO} + \mathrm{N_2} + 2\mathrm{H_2O} \tag{R22}$$

$$\mathrm{CatONH_4} + \mathrm{NO_2(g)} \overset{W_{23}}{\rightarrow} \mathrm{CatONH_2} + \mathrm{NO} + \mathrm{H_2O} \tag{R23}$$

together with their counterparts involving physiosorbed NO_2(s). To reflect the greater reactivity of NO_2 compared to NO in the lower temperature range, the activation energy for each of the two above reactions is taken as $E_{22} = E_{23} = \frac{2}{3}E_{12}$. The pre-exponential factors for these reactions are taken equal to those of reaction R18. The reactions involving physiosorbed NO_2(s) will have zero activation energy and their pre-exponential factors equal one for reaction R19.

Finally, development of this kinetic mechanism is completed with inclusion of further three reactions, the first two for oxidation of the CatONO site with oxygen and the last one for adsorption of NO_2 on the substrate:

$$\mathrm{CatONO} + \mathrm{O_2} \overset{W_{24}}{\rightarrow} \mathrm{CatO} + \mathrm{NO_2(g)} + \mathrm{O(s)} \tag{R24}$$

$$\mathrm{CatONO} + \mathrm{O(s)} \overset{W_{25}}{\rightarrow} \mathrm{CatO} + \mathrm{NO_2(g)} \tag{R25}$$

$$\mathrm{NO_2(g)} + z \overset{W_{26}}{\rightarrow} \mathrm{NO_2(s)} \tag{R26}$$

the rate constants of which are estimated in the same manner as for similar reactions considered above, with the only exception of a lower accommodation factor taken as 0.05 for reaction R26.

The values of the rate constants given in this section were taken as the base line common for all types of catalysts but some adjustments proved necessary in order to achieve quantitative agreement with the measurements used for the assessment of the scheme: this procedure is described below. The complete mechanism with the recommended values of the catalyst-dependent rate constants may be found in the ESI.†

3 Model assessment: numerical implementation

The developed kinetic model is assessed using simulations of a one-dimensional adiabatic plug reactor representing very common micro-reactor experimental setups. The simulated plug flow reactor has a volume of 1 cm^3 and length of 1 cm with its inlet taken as the origin $x = 0$ cm and outlet situated at $x = 1$ cm where x is the direction of the flow. The total amount of catalyst placed in this reactor was taken as 1 g.

The temperature and pressure were constant and for each species an unsteady transport equation was solved for its molar concentration Y neglecting the changes in the density ρ of the gas flow caused by variations of the molecular weight caused by chemical reactions:

$$\frac{\partial Y_i(x,t)}{\partial t} + u\frac{\partial Y_i(x,t)}{\partial x} = R_i \quad (21)$$

where i is the species number, u is the gas flow velocity for the species in the gas phase and $u = 0$ for the surface species and R_i is the total rate of change of the i-th species molar concentration. As the amount of catalyst in the simulations is assumed constant, in order to match conditions of different experiments, u in eqn (21) is taken as the inverse specific residence time, *i.e.* space velocity per unit mass of catalyst. The initial conditions for the surface species were calculated assuming constant total molar surface concentration $n_s = 1.5 \times 10^9$ mole per cm^2 and values of either CatOH or CatO proportional to the molar fraction of catalyst sites. Thus, a catalyst is characterised in this formulation with its specific surface area and catalyst loading only, hence, in order to match the experimental conditions the specific area of this 1 g of catalyst was taken as the total area of catalyst used in the experiments. This procedure ensured that the simulations use exact total molar amounts of active catalytic sites and residence times as used in the experiments chosen for the model assessment.

Eqn (21) was discretised over a grid of N nodes in the x direction using a simple finite volume method with a first-order upwind difference (Patankar);[55] most simulations shown below were conducted with either 100 or 200 nodes; 100 nodes were sufficient to achieve grid independence. Time integration of eqn (21) was performed using SEULEX software implementing an extrapolation algorithm with variable step size based on a linearly implicit Euler method, Hairer and Wanner.[56] The final simulation time was set so as to ensure achievement of stationary outlet gas composition and it was typically of the order of a few thousand seconds. The time step δt for the simulations was set to satisfy the Courant–Friedrichs–Lewy (CFL) condition, $u\delta t < \delta x = 1/(N-1)$, that is the gas flow advanced less than one grid node during one time step.

4 Model assessment: results and discussion

The proposed generic kinetic mechanism was assessed by simulating several experimental studies of SCR operation performed with different catalysts with varying catalyst loading, surface area, feed gas composition, temperatures and GSHV, *i.e.* residence time. The first application has been done for copper-exchanged zeolites, SSZ-13 and SAPO-34 studied by Leistner *et al.*,[43] see Fig. 2–4. These experiments used 30 mg of SSZ with a BET area of 4.39×10^6 cm^2 g^{-1} and 60 mg of SAPO-34 with a BET area of 5.44×10^6 cm^2 g^{-1}, hence, the surface area of the simulated 1 g catalyst, and $\bar{S}$ was set equal to 1.32×10^5 cm^2 for SSZ-13 and 3.26×10^5 cm^2 for SAPO-34. Catalyst loading was determined from the molar ratios of copper to other elements and the initial surface molar fraction of CatO was set to $x_{CatO} = 0.045$ and $x_{CatO} = 0.012$ for SSZ-13 and SAPO-34, respectively. The initial molar fraction of other species was set to zero. The GSHV for both zeolites was given as 30 300 h^{-1} corresponding to the residence time of 0.12 s and the linear gas velocity of $u = 84$ cm s^{-1} for the simulated 1 cm-long catalyst.

Fig. 2 shows the temporal variation of the composition of the gas and concentration of the surface species at the outlet of the Cu/SAPO-34 catalyst at low, medium and high temperature in the range typical of the SCR operation. Clearly, the substrate surface sites have the highest molar concentration, followed by nitrogen. At the initial period, all ammonia but very little NO are adsorbed, and the duration of this transient period depends on the temperature: the longest duration is at medium temperatures corresponding to the optimum SCR conversions. At low temperature, after approximately 500 s, [NH_3] and [NO] at the outlet stabilise at the same value: this demonstrates that the proposed scheme does respect the stoichiometry of the normal SCR conversion. The catalyst sites, initially all in the CatO state, shown as diamonds in Fig. 2, transition to, in order of decreasing concentrations, $CatONH_4$ (shown there as triangles pointing left), Cat (triangles up), $CatONH_2$ (triangles right), and $CatONH_3$ (stars), while the concentrations of CatOH and NH_3(s) are at least two orders of magnitude smaller than the latter and the concentrations of other surface species are negligible. This distribution of the catalytic sites strongly suggests that the redox cycle proceeds through the sequence of reactions R4, R12, R1 and R6, with the oxidation step concluding the cycle in reactions R8 and R15. Large amounts of $CatONH_4$ and Cat indicate that either reaction R8 or reaction R6 is a limiting step for the entire cycle; the combination of NO conversion well below 100% and abundance of molecular oxygen suggests that the rate limitation is caused by the slowness of the chemical reaction rather than mass transfer. Hence, under these conditions the rate of conversion will scale linearly with the catalyst loading or total amount and inversely with the residence time.

The reaction sequence suggested above for the low temperature is corroborated with the calculation of the reaction rates shown in Fig. 3. It is seen that the rates of formation of ammonium and physisorption of ammonia are much larger than the rates of the reactions in the redox cycle and they therefore are equilibrated with their reverse reactions of desorption. The reactions of the main redox cycle, see the figure in the top right of Fig. 3, have progressively diminishing, but approximately the same, rates: reaction R12 (triangles right), reaction R4 (bold dotted line), reaction R6 (large circles), but the oxidation reaction R8 producing surface atomic oxygen is much slower; reaction R15 consuming O(s) is slower still. Thus, for this low temperature the catalyst re-oxidation is the limiting step.

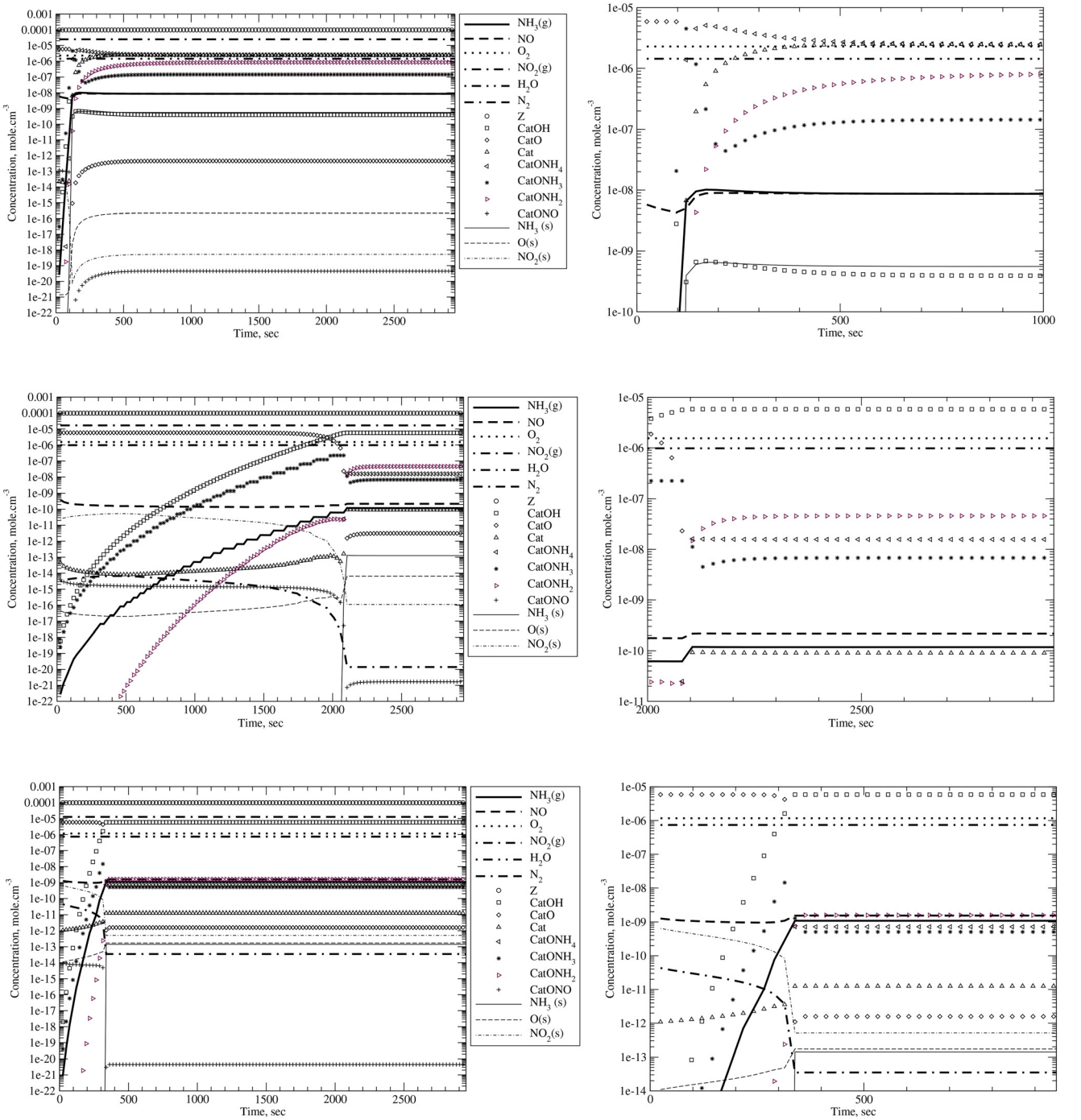

Fig. 2 Transient composition of the gas and concentration of the surface species at the outlet of the Cu/SAPO-34 catalyst in SCR operation at 150 °C (top), 350 °C (middle), 550 °C (bottom). The inserts on the right show the magnified period around achieving the steady-state operation. The notation is the same as on the main figure on the left. The inlet gas composition is: $x_{NO} = x_{NH_3}$ = 400 ppm, x_{O_2} = 8%, x_{H_2O} = 5% with the rest being N_2. The inlet gas velocity is 8.4 cm s^{-1}.

Returning to the concentration of species shown in Fig. 2, one may see that the temperature increase to 350 °C resulted in a very large increase of CatOH (squares) and a very strong decrease in concentration of Cat (triangles up) thus indicating that now the active site reduction reaction R6 is gradually replacing oxidation as the redox cycle limiting step. Indeed, this is confirmed by direct comparison of the rates: reaction R6 (large circles) and reaction R8 (straight crosses) now proceed at the same rate, noticeably slower than other parts of the redox pathway operational at low temperatures. As may be expected, the rate of every individual step is very much increased with the temperature rise, however, it is noticeable that the reaction rates in a steady-state operation decrease significantly, by nearly three orders of magnitude towards the catalyst exit; a

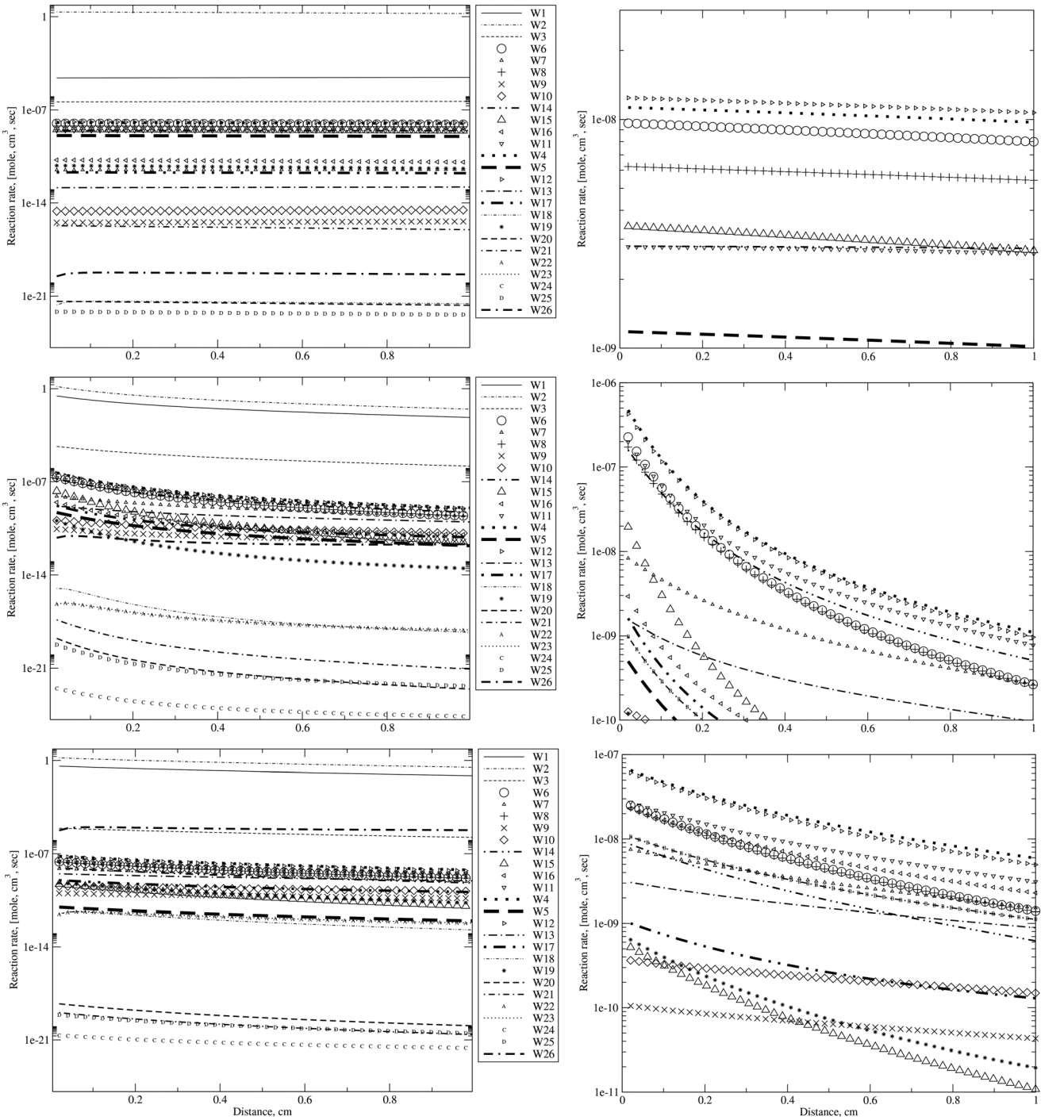

Fig. 3 Reaction rates in established steady-state SCR operation along the length of the Cu/SAPO-34 catalyst at 150 °C (top), 350 °C (middle), 550 °C (bottom). The inserts on the right discern the main redox cycle reaction rates with exception of reaction R1: the notation is the same as on the main figure on the left. The inlet gas composition is: $x_{NO} = x_{NH_3}$ = 400 ppm, x_{O_2} = 8%, x_{H_2O} = 5% with the rest being N_2. The inlet gas velocity is 8.4 cm s^{-1}.

simple explanation to this fact is that the overall amount and increased reactivity of the active sites at this temperature consume most of the ammonia closer to the inlet, thus one may safely assume that under these conditions the conversion rate close to 100% may be maintained even for considerably larger gas debits, *i.e.* much smaller residence times. Finally, it should be noticed that now much faster oxidation step reaction R8 produces amounts of O(s) sufficient to trigger a second alternative redox pathway proceeding with oxidation of $CatONH_4$ *via* reaction R14 (dash-dot-dot line) and resulting in the rate of reduction *via* reaction R11 comparable with the total conversion rate of the low temperature cycle.

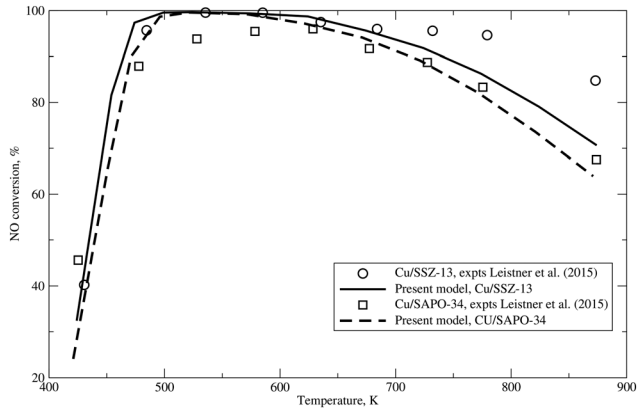

Fig. 4 NO conversion *vs.* temperature for two copper-exchanged zeolites for SCR operation. The inlet gas composition is: $x_{NO} = x_{NH_3}$ = 400 ppm, x_{O_2} = 8%, x_{H_2O} = 5% with the rest being N_2. The inlet gas velocity is 8.4 cm s^{-1}. Symbols are measurements of Leistner *et al.*[43]

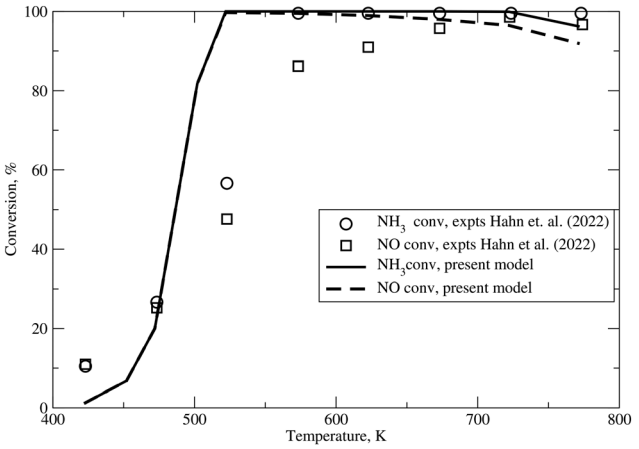

Fig. 5 NH_3 and NO conversion *vs.* temperature for SCR operation with Fe-exchanged HBEA zeolite, Hahn *et al.*[14] The inlet gas composition is: $x_{NO} = x_{NH_3}$ = 500 ppm, x_{O_2} = 5%, with the rest being N_2. The inlet gas velocity is 15.3 cm s^{-1}, $\bar{S} = 2.46 \times 10^6$ cm^2, the initial catalyst loading is x_{CatO} = 0.008. Symbols are measurements of Hahn *et al.*[14]

Further temperature increase to 550 °C, see the bottom row of Fig. 2 and 3, leads to sub-optimal SCR operation with the NO conversion rate decreasing by more than 20%, see Fig. 4. The concentration of the active states in the intermediate states $CatONH_4$, $CatONH_3$ and $CatONH_2$ drops by two orders of magnitude compared with the case of 350 °C: this indicates that the redox cycle rate is now limited by the ammonia desorption and ammonium dissociation with the equilibrium of both reactions R1 and R2 shifted to the left. In principle, temperature increase may slow down the low-temperature redox cycle, owing to the equilibrium of reaction R17 and R18 shifted to the left, but this factor is not important under the investigated conditions. Thus, the overall efficiency of SCR conversion does not seem to have a single limiting factor, and the changing competition between the different pathways may, at least qualitatively, explain the "sea-gull shape" of the efficiency dependency upon temperature for a given catalyst, Gao *et al.*[57]

Comparing predictions of this mechanism with the measurements of Leistner *et al.*,[43] see Fig. 4, one may see that SSZ-13 exhibits a drop of SCR efficiency at high temperatures smaller than SAPO-34 does; while differences in catalyst loading and the surface explain a part of this difference, *cf.* solid and dashed lines in Fig. 4, a noticeable difference remains. Both zeolites are copper-exchanged, thus the reason is unlikely to be related to the reactivity of the active sites. Based on predictions of the present model, one may suggest that the very likely reason for this difference is that SSZ-13 has a slightly larger activation barrier to weakly bound ammonia desorption: a modest increase of activation energy of reverse reaction R2 allows a very good match of the SCR efficiency (not shown) observed with this zeolite.

One of the base assumptions in the development of this mechanism was that different active catalytic sites may be characterised with the same rate constants; while this assumption is very convenient for estimation of rate constants, it is clearly inaccurate: as may be seen from Fig. 5, the SCR conversion observed for Fe-exchanged zeolite is much worse at low temperatures than that for Cu-exchanged ones considered previously and simulations with the rate constants of the base model (not shown) overpredict the performance for the temperatures below 300 °C in comparison with measurements of Hahn *et al.*[14] These measurements employed a reactor with a much larger total catalyst amount, and hence, a total area of 2.46×10^6 cm^2, catalyst loading x_{CatO} = 0.008 and twice larger GSHV, yielding a linear feed velocity of u = 15.3 cm s^{-1}, the value matching their residence time. The higher amount of catalyst sites may explain the superior performance at temperatures of 450 °C and above, but it cannot account for poor low-temperature conversion; thus, the question arises of how many alterations are required for the base mechanism to represent this type of catalyst. According to the above rate analysis, the conversion rate at low temperatures is limited by reaction R8, therefore, the rate of the latter is the defining factor for the degree of conversion. It proved that the increase of the activation energy of this reaction from 80 to 95 kJ per mole brings the low-temperature conversion for Fe-exchanged zeolite into the correct range, see Fig. 5. While the agreement is not ideal, it is remarkable that a change of a single kinetic parameter allows one within the present kinetic mechanism to reconcile iron and copper zeolite-based catalysts.

Compared to zeolites, catalysts on the TiO_2 substrate, such as vanadia–tungsta ones, have much smaller specific surface areas, hence, for comparable catalyst loading, they have smaller concentration of active sites, yet they are widely used when the size of the SCR converter is not very important, *e.g.* in marine and power generation applications. Two such catalysts, CeO_2 and V_2O_5 on the TiO_2 substrate, were simulated here for conditions of experiments of Huang *et al.*[58] and the outcomes are shown in Fig. 6. For V_2O_5 the experimental conditions were matched with the simulated catalyst area of $\bar{S} = 5.89 \times 10^4$ cm^2, catalyst loading of x_{CatOH}

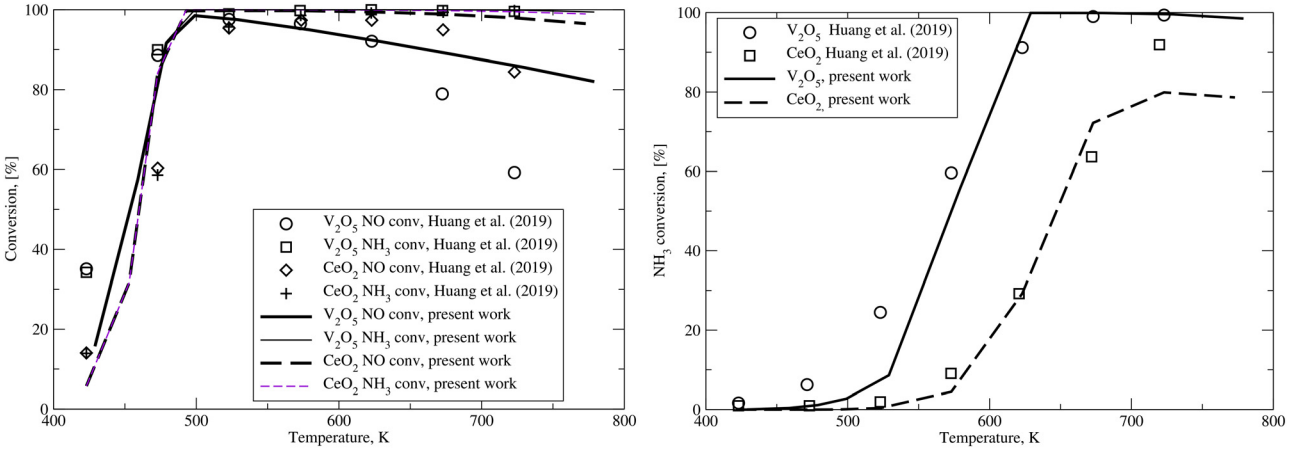

Fig. 6 Left: NH_3 and NO conversion *vs.* temperature for SCR operation of two catalysts, CeO_2 and V_2O_5, on a tungsta substrate. Right: NH_3 conversion *vs.* temperature for the same catalysts for ammonia oxidation. The inlet gas composition is for SCR: $x_{NO} = x_{NH_3}$ = 500 ppm, for ammonia oxidation x_{NH_3} = 500 ppm, with x_{O_2} = 2% with the rest being N_2 for both cases. The inlet gas velocity is 3.3 cm s^{-1}. Symbols are measurements of Huang *et al.*[58]

= 0.03 and for CeO_2: $\bar{S} = 1.26 \times 10^5$ cm^2 with $x_{CatOH} = 0.1$, *i.e.* the latter had approximately 6 times more active sites. Similar to Fe-exchanged zeolite, and despite the relatively high active site concentration, the cerium dioxide catalyst exhibits poor low-temperature conversion for both SCR operation and NH_3 oxidation not captured with the baseline set of rate constants. However, as it was the case with the Fe-exchanged zeolite, the increase of the activation energy for reaction R8 to 90 kJ per mole has allowed a reasonably good agreement to be achieved with the measurements of Huang *et al.*[58] with the exception of ammonia oxidation at 450 K underpredicted by approximately 10%.

Of all the catalysts simulated so far, the vanadia–tungsta on titania one of Huang *et al.*[58] has the lowest surface and active site concentration and the highest residence time; at higher temperatures the measurements showed a significant decrease of NO conversion, while the NH_3 consumption remained nearly complete. The baseline set of the rate constants showed in this case a good agreement at lower temperatures, but at high temperatures the predicted conversion of both NO and NH_3 was smaller than those measured for both SCR and NH_3 oxidation. The reaction rate analysis showed that in this case the high temperature redox pathway proceeding through oxidation of $CatONH_2$, rather than the Cat intermediate see Fig. 1, was very slow. Therefore, activation energies for reactions R7 and R9 were decreased to 85 and 95 kJ per mole, respectively; the results are shown in Fig. 6. While this change allowed one to obtain a fairly good agreement for NH_3 conversion under all conditions, the present kinetics still overpredicted NO conversion at temperatures above 400 °C. The diverging degrees of ammonia and nitric oxide conversion were, however, shown in Huang *et al.*[58] to be caused by the formation of nitrous oxide N_2O, the detailed mechanism of which has so far not been considered in SCR chemical kinetic mechanisms. Clearly, inclusion of the chemical pathways for nitrous oxide formation would be a desirable next step in the development of SCR kinetic schemes. Another aspect well worthy of comment and a further investigation is representation of the role of water in the exhaust gas.

The current formulation assumes that the water in the exhaust or flue gas is chemically inert; it is formed as a product in the redox cycles but its concentration does not affect the reaction rates. At the same time, there does exist experimental evidence that water concentration in the gas phase affects the SCR reaction rates. Work of Nova *et al.*[59] demonstrated that addition of up to 5% vol. of H_2O decreases SCR conversion efficiency in a vanadia–tungsta catalyst but it does not affect the rates of NH_3 adsorption or desorption. Because of this it was argued that its role cannot be reduced to surface coverage competition. DFT simulations of Broclawik *et al.*[60] of the same type of catalyst demonstrated the possibility of low temperature water dissociation leading to the formation of active hydroxyls bound to tungsten ions; however, this process creates stronger Brønsted sites and thus it should promote rather than inhibit SCR conversion. This finding explains that addition of tungsta to vanadia catalysts significantly improves low-temperature SCR performance but it does not explain the inhibiting effect of increasing water concentration in the flue gas to be scrubbed. At the same time, addition of a fixed amount of water markedly increased NO conversion in several Cu-exchanged zeolites at higher, above 400 °C, temperatures, Fedyna *et al.*,[61] while at lower, between 100 and 200 °C, temperatures water could inhibit, promote or leave the conversion unchanged. The promotion of catalytic activity was attributed to transition of isolated copper ions and their dimers to Cu^{2+}–OH^- centres, Fedyna *et al.*,[61] as confirmed spectroscopically. The proposed mechanism does have distinct low and high-temperature pathways but the question to which extent reactions on the different structures with copper cations may be lumped together in the adopted generalised kinetics scheme should at

present be considered open. It is worth mentioning that formation of metal-hydroxyl groups was associated with the N_2O reactions in DFT simulations of Song *et al.*[62] performed for a Mn-doped ceria catalyst thus indicating that the N_2O and H_2O pathways should be considered together in the subsequent developments of this, or indeed, any other kinetic scheme for SCR catalysts.

5 Conclusions

It is remarkable that a patently wrong departure point, namely assuming the same reactivity for different SCR catalytic sites, has proved rather fruitful in allowing to develop a new generic chemical kinetic scheme aimed at exploiting similarities in reduction–oxidation catalytic cycles for nitric oxide reduction to nitrogen by ammonia. This generic scheme comprises 28 reactions involving 16 species where a catalytically active site may be in 7 states. The rate constants for these reactions were estimated through analysis of the individual sub-processes and identifying the overall rate with the rate of the limiting sub-process. The chemical kinetics so developed was used to simulate operation of several catalysts through matching catalyst concentration and residence times. These simulations show that, after taking into account differences in feed gas composition, active site concentration and residence time, varying only one kinetic parameter, namely activation energy for the low-temperature pathway allows one to reconcile the observed differences between copper and iron exchanged zeolites and cerium dioxide on tungsta. These simulations show that it is plausible that differences in the operating regime of a catalytic converter matter at least as much as the nature of the catalyst sites.

In what concerns the development of this chemical kinetics, vanadia on TiO_2 appears different from other catalysts as achieving a similar agreement of its simulations with the observed rates of SCR conversion required changes of activation energy of two high-temperature active site oxidation reactions. Its simulations have also identified pathway(s) of nitrous oxide formation as essential for description of its high-temperature behaviour and consideration of effects of addition of water to the gas to be scrubbed indicates that this pathway should be considered alongside water adsorption and dissociation on the catalyst surface.

Data availability

The developed chemical kinetic mechanism and its rate constants are supplied in CHEMKIN format as the ESI.† The simulation data and the code are available upon request.

Author contributions

AAB: kinetic mechanism formulation, simulations and manuscript, APM: simulations and manuscript.

Conflicts of interest

There are no conflicts of interest to declare.

Acknowledgements

APM acknowledges the financial support through RDF studentship from Northumbria University.

References

1 L. Han, S. Cai, M. Gao, J. Y. Hasegawa, P. Wang, J. Zhang, L. Shi and D. Zhang, *Chem. Rev.*, 2019, **119**, 10916–10976.
2 Z. Lian, Y. Li, W. Shan and H. He, *Catalysts*, 2020, **10**, 1421.
3 T. V. W. Janssens, H. Falsig, L. F. Lundegaard, P. N. R. Vennestrøm, S. B. Rasmussen, P. G. Moses, F. Giordanino, E. Borfecchia, K. A. Lomachenko, C. Lamberti, S. Bordiga, A. Godiksen, S. Mossin and P. Beato, *ACS Catal.*, 2015, **5**, 2832–2845.
4 N. Y. Topsøe, J. A. Dumesic and H. Topsøe, *J. Catal.*, 1995, **151**, 241–252.
5 L. Olsson, K. Wijayanti, K. Leistner, A. Kumar, S. Y. Joshi, K. Kamasamudram, N. W. Currier and A. Yezerets, *Appl. Catal., B*, 2016, **183**, 394–406.
6 U. De-La-Torre, B. Pereda-Ayo, M. Gutiérrez-Ortiz, J. González-Marcos and J. González-Velasco, *Catal. Today*, 2017, **296**, 95–104.
7 D. Chatterjee, T. Burkhardt, B. Bandl-Konrad, T. Braun, E. Tronconi, I. Nova and C. Ciardelli, *SAE Technical Papers 2005-01-0965*, 2005.
8 E. D. German and M. Sheintuch, *Russ. J. Phys. Chem. B*, 2007, **1**, 357–376.
9 L. Arnarson, H. Falsig, S. B. Rasmussen, J. V. Lauritsen and P. G. Moses, *J. Catal.*, 2017, **346**, 188–197.
10 M.-J. Kim, J.-R. Youn, S.-J. Lee, I.-S. Ryu, S. Chan Nam, S. Kwan Jeong and S. Goo Jeon, *J. Ind. Eng. Chem.*, 2022, **108**, 438–448.
11 Q. Jin, M. Chen, X. Tao, B. Lu, J. Shen, Y. Shen and Y. Zeng, *Appl. Surf. Sci.*, 2020, **512**, 145757.
12 M. Ravi, V. L. Sushkevich and J. A. van Bokhoven, *Chem. Sci.*, 2021, **12**, 4094–4103.
13 Z. Ma, X. Wu, H. Härelind, D. Weng, B. Wang and Z. Si, *J. Mol. Catal. A: Chem.*, 2016, **423**, 172–180.
14 C. Hahn, J. Seidel, F. Mertens and S. Kureti, *Phys. Chem. Chem. Phys.*, 2022, **24**, 7493–7504.
15 M. Inomata, A. Miyaoto and M. Yuichi, *J. Catal.*, 1980, **62**, 140–148.
16 L. Arnarson, H. Falsig, S. B. Rasmussen, J. V. Lauritsen and P. G. Moses, *Phys. Chem. Chem. Phys.*, 2016, **18**, 17071.
17 G. Busca, L. Lietti, G. Ramis and F. Berti, *Appl. Catal., B*, 1998, **18**, 1–36.
18 V. Zhdanov, *Elementary physico-chemical processes on a surface,* "*Nauka*", Siberian Section, Novosibirsk, 1988.
19 L. Lietti, G. Ramis, F. Berti, G. Toledo, D. Robba, G. Busca and P. Forzatti, *Catal. Today*, 1998, **42**, 101–116.
20 L. J. Alemany, L. Lietti, N. Ferlazzo, P. Forzatti, G. Busca, E. Giamello and F. Bregani, *J. Catal.*, 1995, **155**, 117–130.

21 D. Chatterjee, T. Burkhardt, M. Weibel, I. Nova, A. Grossale and E. Tronconi, *SAE Technical Papers 2007-01-1136*, 2007, vol. 2007.
22 V. Schmeisser, M. Weibel, L. Sebastian Hernando, I. Nova, E. Tronconi and M. P. Ruggeri, *SAE Int. J. Commer. Veh.*, 2013, **6**, 190–199.
23 C. T. Campbell, L. Árnadóttir and J. R. Sellers, *Z. Phys. Chem.*, 2013, **227**, 1435–1454.
24 N. B. Vargaftik, *Handbook of Physical Properties of Liquids and Gases, Pure Substances and Mixtures*, Springer-Verlag Berlin Heidelberg, 2nd edn, 1975.
25 M. Colombo, I. Nova, E. Tronconi, V. Schmeißer, B. Bandl-Konrad and L. Zimmermann, *Appl. Catal., B*, 2012, **111–112**, 106–118.
26 T. Masuda, Y. Fujikata, H. Ikeda, S. Matsushita and K. Hashimoto, *Appl. Catal., A*, 1997, **162**, 29–40.
27 U. Diebold and T. E. Madey, *J. Vac. Sci. Technol., A*, 1992, **10**, 2327–2335.
28 H. E. Dastoor, P. Gardner and D. A. King, *Surf. Sci.*, 1993, **289**, 279–289.
29 L. Ye, B. T. Lo, J. Qu, I. Wilkinson, T. Hughes, C. A. Murray, C. C. Tang and S. C. E. Tsang, *Chem. Commun.*, 2016, **52**, 3422–3425.
30 I. Chorkendorff and J. Niemanrsverdriet, *Concepts of modern catalysis and kinetics*, Wiley-VCH Verlag, Weinheim, 2nd edn, 2007.
31 S. Suárez, S. Jung, P. Avila, P. Grange and J. Blanco, *Catal. Today*, 2022, **75**, 331–338.
32 X. Yin, H. Han, I. Gunji, A. Endou, S. S. Cheettu Ammal, M. Kubo and A. Miyamoto, *J. Phys. Chem. B*, 1999, **103**, 4701–4706.
33 A. Marberger, D. Ferri, M. Elsener and O. Kröcher, *Angew. Chem., Int. Ed.*, 2016, **55**, 11989–11994.
34 J. J. Scholten, P. Zwietering, J. A. Konvalinka and J. H. De Boer, *Trans. Faraday Soc.*, 1959, **55**, 2166–2179.
35 M. Fan, H. Panezai, J. Sun, S. Bai and X. Wu, *J. Phys. Chem. C*, 2014, **118**, 23761–23767.
36 M. A. Henderson, *Surf. Sci.*, 1994, **319**, 315–328.
37 V. Y. Prokof'ev, N. E. Gordina, T. N. Borisova and N. V. Shamanaeva, *Microporous Mesoporous Mater.*, 2019, **280**, 116–123.
38 A. Feng, B. J. McCoy, Z. A. Munir and D. E. Cagliostro, *J. Colloid Interface Sci.*, 1996, **180**, 276–284.
39 Y. Cheng, W. Song, J. Liu, H. Zheng, Z. Zhao, C. Xu, Y. Wei and E. J. M. Hensen, *ACS Catal.*, 2017, **7**, 3883–3892.
40 I. Nova, C. Ciardelli, E. Tronconi, D. Chatterjee and M. Weibel, *AIChE J.*, 2009, **55**, 1514–1529.
41 Z. Ma, X. Wu, H. Härelind, D. Weng, B. Wang and Z. Si, *J. Mol. Catal. A: Chem.*, 2016, **423**, 172–180.
42 M. Koebel, G. Madia and M. Elsener, *Catal. Today*, 2002, **73**, 239–247.
43 K. Leistner, O. Mihai, K. Wijayanti, A. Kumar, K. Kamasamudram, N. Currier, A. Yezerets and L. Olsson, *Catal. Today*, 2015, **258**, 49–55.
44 L. Sivachandiran, F. Thevenet, P. Gravejat and A. Rousseau, *Appl. Catal., B*, 2013, **142–143**, 196–204.
45 R. S. Ghosh, M. P. Harold and D. Wang, *Chem. Eng. J.*, 2021, **418**, 129065.
46 M. Crocoll, S. Kureti and W. Weisweiler, *J. Catal.*, 2005, **229**, 480–489.
47 R. Villamaina, U. Iacobone, I. Nova, E. Tronconi, M. P. Ruggeri, L. Mantarosie, J. Collier and D. Thompsett, *Appl. Catal., B*, 2021, **284**, 119724.
48 M. Ambast, A. Gupta, B. M. M. Rahman, L. C. Grabow and M. P. Harold, *Appl. Catal., B*, 2021, **286**, 119871.
49 T. Wentworth, S. Loya, C. Depcik and S. Susan Stagg-Williams, *React. Kinet., Mech. Catal.*, 2016, **117**, 15–34.
50 J. Despres, M. Koebel, O. Kröcher, M. Elsener and A. Wokaun, *Microporous Mesoporous Mater.*, 2003, **58**, 175–183.
51 P. Treesukol, J. Limtrakul and T. N. Truong, *J. Phys. Chem. B*, 2001, **105**, 2421–2428.
52 R. Baetzold and G. Somorjai, *J. Catal.*, 1976, **45**, 94–105.
53 N. Zhanpeisov, H. Nakatsuji, M. Hada, H. Nakai and M. Anpo, *Catal. Lett.*, 1996, **42**, 173–176.
54 N. Wilken, K. Kamasamudram, N. Currier, J. Li, A. Yezerets and L. Olsson, *Catal. Today*, 2010, **151**, 237–243.
55 S. Patankar, *Numerical Heat Transfer and Fluid Flow*, Hemisphere Publ, Washington D.C., 1980.
56 E. Hairer and G. Wanner, *Solving ordinary differential equations II. Stiff and differential-algebraic problems. Springer series in computational mathematics 14*, Springer-Verlag, Berlin, 2nd edn, 1996.
57 F. Gao, E. D. Walter, M. Kollar, Y. Wang, J. Szanyi and C. H. Peden, *J. Catal.*, 2014, **319**, 1–14.
58 N. Huang, Y. Geng, S. Xiong, X. Huang, L. Kong, S. Yang, Y. Peng, J. Chen and J. Lia, *Catal. Commun.*, 2019, **121**, 84–88.
59 I. Nova, L. Lietti, E. Tronconi and P. Forzatti, *Catal. Today*, 2000, **60**, 73–82.
60 E. Broclawik, A. Góra and M. Najbar, *J. Mol. Catal. A: Chem.*, 2001, **166**, 31–38.
61 M. Fedyna, P. Legutko, M. Marzec and Z. Sojka, *Appl. Catal., B*, 2025, **361**, 124632.
62 W. Song, J. Liu, H. Zheng, S. Ma, Y. Wei, A. Duan, G. Jiang, Z. Zhao and E. J. M. Hensen, *Catal. Sci. Technol.*, 2016, **6**, 2120–2128.

